This is a preprint, the final version is subject to change, of the American Mineralogist (MSA)
Cite as Authors (Year) Title. American Mineralogist, in press.
DOI: https://doi.org/10.2138/am-2019-6823

Revision 2

Title:

Phase transition of wadsleyite-ringwoodite in the Mg_2SiO_4-Fe_2SiO_4 system

Authors:

[1,*]Noriyoshi Tsujino, [1]Takashi Yoshino, [1]Daisuke Yamazaki, [1,2]Moe Sakurai, [1]Wei Sun, [1]Fang Xu, [3]Yoshinori Tange, [3]Yuji Higo

Affiliations:

[1]Institute for Planetary Materials, Okayama University, 827 Yamada, Misasa, Tottori 682-0193, Japan.

[2]Department of Earth and Planetary Sciences, Tokyo Institute of Technology, 2-12-1 Ookayama, Meguro, Tokyo 152-8551, Japan

[3]Japan Synchrotron Radiation Research Institute, 1-1-1 Kouto, Sayo, Hyogo 689-5198, Japan.

Corresponding author: tsujino@okayama-u.ac.jp

Keywords: mantle, wadsleyite, ringwoodite, phase boundary loop, in-situ experiments

This is a preprint, the final version is subject to change, of the American Mineralogist (MSA)
Cite as Authors (Year) Title. American Mineralogist, in press.
DOI: https://doi.org/10.2138/am-2019-6823

Abstract

The Fe-bearing wadsleyite-ringwoodite phase transition loop under dry conditions in a temperature range of 1473 and 1873 K was determined by in-situ X-ray diffraction experiments at the synchrotron facility SPring-8. Pressure at high temperature was precisely determined within a 0.23 GPa error using in-situ X-ray diffraction of MgO as a pressure standard. Under dry conditions, assuming an equilibrium chemical composition of wadsleyite and ringwoodite coexisting with garnet in a pyrolite model and an adiabatic temperature gradient with a potential temperature of 1550–1650 K, the phase transition depth and effective width of the seismic discontinuity were found to be 500–514 km and 20–22 km, respectively. This effective width, which is three times greater than that of the olivine-wadsleyite phase boundary, can reflect a seismic wave of approximately 0.25 Hz. The wider transition loop between wadsleyite and ringwoodite could create a broad seismic discontinuity. Considering wet and oxidized conditions, the depth of the wadsleyite-ringwoodite phase boundary could be greater than 520 km assuming the small temperature dependency on water and oxygen fugacity effects. Variation in the depth of seismic anomaly may be attributed to water content or oxygen fugacity of the transition zone.

Introduction

Various seismic discontinuities in the Earth's interior have been globally determined by various seismic studies (e.g., Dziewonski and Anderson, 1981). Phase transitions in the major constituent minerals are believed to cause such global discontinuities in the Earth's mantle. According to the velocity model (IASP91) proposed by Kennett and Engdahl (1991), an increase in P and S wave velocities by 3.6% and 4.1%, respectively, can be explained by the olivine-wadsleyite phase transition at 410-km seismic discontinuity. The post-spinel phase transition accounts for the 660-km seismic discontinuity characterized by P and S wave velocity increases of 5.8% and 6.3%, respectively. However, the phase transition between wadsleyite and ringwoodite produces velocity increases of only 1% or less (Helfflich, 2000). Although several seismic studies using long period seismograms have suggested that the 520-km seismic discontinuity is a global feature (e.g., Shearer, 1990, 1991; Flanagan and Shearer, 1998), recent seismic studies demonstrated that this discontinuity is not a ubiquitous feature and is lacking in some regions (Gossler and Kind, 1996; Deuss and Woodhouse, 2001). In some cases, two discontinuities at approximately 500- and/or 560-km depths were detected rather than the 520-km seismic discontinuity (Deuss and Woodhouse, 2001). Therefore, to understand the nature of the 520-km seismic discontinuity, it is important to accurately determine the phase boundary between wadsleyite and ringwoodite as a function of temperature, pressure, and chemical composition.

Temperature is among the key parameters that constrain the structure and composition of the

Earth's interior. Although geophysical observations allow for the precise determination of depth, and hence, pressure, it is difficult to determine the temperature at a given depth without knowledge of mineral physics. The combined studies of potential temperature (e.g., McKenzie and Bickle, 1988), phase boundary depth of constituent minerals, and depth of seismic discontinuities (Akaogi et al., 1989; Katsura et al., 2004) have made it possible to estimate a temperature profile of the Earth's mantle. The phase boundary binary loop between wadsleyite and ringwoodite is among the most important interfaces of the major predicted phase transitions used to constrain the mantle geotherm.

Using in-situ X-ray diffraction at a synchrotron facility, Morishima et al. (1994) and Katsura et al. (2004) determined the olivine-wadsleyite phase boundary in the Mg-endmember and Fe-bearing systems, respectively. The phase boundary between wadsleyite and ringwoodite has only been determined in the Mg-endmember system by in-situ studies (Inoue et al., 2006; Suzuki et al., 2000), while the phase boundary loop of wadsleyite-ringwoodite in Fe-bearing systems has only been estimated through thermodynamic calculations (Akaogi et al, 1989; Frost 2003) and quench experiments (e.g., Katsura and Ito, 1989). In this study, we determined the precise pressure of the phase boundary loop between wadsleyite and ringwoodite at various temperatures under dry conditions via in-situ high-pressure experiments. We also discuss the origin of the 520-km seismic discontinuity based on the wadsleyite-ringwoodite phase transition.

Experimental methods

In-situ X-ray diffraction experiments were conducted using a Kawai-type multi-anvil apparatus SPEED-1500 installed at the beamline BL04B1 of the synchrotron facility SPring-8 (Utsumi et al., 1998). The pressure medium was an octahedron composed of 5 wt.% Cr_2O_3 doped MgO with an edge length of 10 mm. The pressure medium was compressed using tungsten-carbide anvils with 4- or 5-mm truncated edge lengths. Olivine with a composition of $(Mg_x,Fe_{1-x})_2SiO_4$, where x = 0.97, 0.91, 0.80, and 0.70, was used as a starting material. For x = 0.91, natural olivine from San Carlos, Arizona, U.S.A. was used. Other olivine compositions were synthesized using oxide powders, which were also used by Katsura et al. (2004). A powder mixture composed of MgO with 10 wt.% Pt, or 20 wt.% h-BN only for S3323, to suppress grain growth, was used as a pressure marker. Figure 1 shows the design of the cell assembly for the in-situ X-ray diffraction experiments at high pressures and temperatures. Two samples with different Fe contents and a pressure marker, separated by Mo foils (30 μm), were packed into a graphite capsule. Oxygen fugacity was controlled to be similar to the Mo-MoO_2 buffer, which is near to that of the Fe-FeO buffer, using a Mo foil inside the graphite capsule. The thickness of each sample and the pressure marker was ~300 μm. A cylindrical TiB_2 + BN + AlN composite (with 2.6 and 2.0 mm outer and inner diameter, respectively, and 6.3 mm in length) was used as a heater. Cylindrical $LaCrO_3$ was used as a thermal insulator surrounding the heater. The temperature difference between the center and edge of the capsule was estimated to be approximately 50 K by the compositional difference (Mg# = Mg / (Mg + Fe) × 100) of the wadsleyite and ringwoodite of S3255 and 5K3134, assuming that the pressure was constant in

the graphite capsule. Therefore, the maximum temperature difference was less than 50 K around the cylindrical X-ray window composed of the MgO placed in the thermal insulator. The temperature was monitored by a W3%Re-W25%Re thermocouple, whose junction was sandwiched between the MgO disks 0.2 mm in thickness adjacent to the pressure marker, to minimize the temperature difference between the thermocouple junction and the pressure marker, for a precise pressure calculation using the equation of state of MgO. The maximum temperature difference estimated at the pressure marker position was 25 K, corresponding to a pressure difference of 0.16 GPa, when we used the equation of the state of MgO proposed by Tange et al. (2009).

A solid-state detector connected to a multi-channel analyzer was used to collect the X-ray diffraction data. The energy was calibrated with the characteristic X-rays of Pb, Au, Pt, Ta, Ag, Mo, and Cu or the γ-ray of ^{55}Fe, ^{57}Co, and ^{133}Ba. The diffracted X-rays from the sample and pressure marker were collected at a fixed 2θ angle of 6° using the energy-dispersive method. The 2θ angle was calibrated using the MgO unit-cell volume in the pressure marker calculated by the (111), (200), (220), (311), and (222) diffraction peaks at ambient conditions except for Run No. S3323. During Run No. S3323, the (111), (220), (311), (222), and (400) diffraction peaks of MgO were used to calibrate the 2θ angle because the (200) diffraction peak overlapped with that of cubic-BN at a high pressure and temperature. Errors in the pressure calculation were recorded as deviations in the individual peak positions, which were a maximum of 0.23 GPa and an average of 0.16 GPa. The sample was compressed to a desired pressure and then heated to a desired temperature (see Table 1).

To establish the chemical equilibrium between wadsleyite and ringwoodite, the desired temperature was maintained for 1 to 8 h (see Table 1). Generally, after the desired temperature is reached, the pressure slightly decreases (e.g., Nishiyama et al., 2004). To confirm the chemical equilibrium in the samples after settling the pressure by a different pressure-temperature path, in S3323 the pressure was maintained at a higher level than that immediately after the desired temperature was reached by additional compression. The X-ray diffraction data were collected from the pressure marker immediately before quenching, to determine the precise pressure at high temperatures. The pressure was determined using the third-order Birch-Murnaghan equation of state (3BM) of MgO proposed by Tange et al. (2009) and Speziale et al. (2001).

To confirm the chemical equilibrium between wadsleyite and ringwoodite, additional quench experiments using the same cell assembly as the in-situ experiments were conducted at ~14 GPa and 1673 K for 1 h. Two samples were set in the same run; one being an olivine powder with a composition of $x = 0.80$ which was the same as that used in in-situ experiments, and the other a mixture of olivine powder of $x = 0.97$ and 0.70 with a bulk composition of $x = 0.80$. At a high pressure and temperature, wadsleyite and ringwoodite were formed by the decomposition of the olivine powder with $x = 0.80$, while these were formed by reverse reaction from the mixture of olivine powder with $x = 0.97$ and $x = 0.70$.

After the annealing experiments, the recovered samples were mounted in an epoxy resin and polished with diamond paste (1 μm in grain size). The chemical compositions of the coexisting

wadsleyite and ringwoodite were measured using an electron probe micro-analyzer. (EPMA, JEOL-8800) combined with wavelength dispersion spectroscopy (WDS) at the Institute for Planetary Materials, Okayama University. An accelerating voltage and a beam current of 15 kV and 1.2×10^{-8} A, respectively, were applied at an interval of 20 s for the peak and 10 s for the background signals. For each phase in recovered samples, typically 5 or more chemical compositional measurements were conducted at various positions. The standards for quantitative analyses of the sample composition were periclase, hematite, and wollastonite for MgO, FeO, and SiO_2, respectively. All the measurements were validated with reference to olivine

Results and discussions

Experimental conditions and results of the in-situ X-ray diffraction are summarized in Table 1. High-pressure experiments were conducted at 1473–1873 K and 12.6–18.0 GPa using the MgO scale of Tange et al. (2009). Figure 2 shows typical backscattered electron images of the recovered samples synthesized at 1473–1873 K. There was no heterogeneity in the chemical composition of each phase (wadsleyite and ringwoodite) obtained from each experiment. The partitioning coefficient K_D values of Fe and Mg between wadsleyite and ringwoodite, following $K_D = \left(X_{Fe}^{Wd}/X_{Mg}^{Wd}\right)/\left(X_{Fe}^{Rw}/X_{Mg}^{Rw}\right)$, are nearly identical at 1673 K regardless of the composition, starting material type, and run duration (1 to 8 h) including the quench experiments (see Figure 3 and Table 1). Inoue et al. (2010a, b) also determined the phase relation of olivine composition in dry and wet

154 systems by quench experiments at 1673 K. The K_D determined by Inoue et al. (2010a, b) is
155 consistent with that determined in this study. At 1873 K, chemical equilibrium was achieved faster
156 than at 1673 K. The diffusion coefficients for wadsleyite and ringwoodite at 1473 K are three to
157 four times lower than those at 1673 K based on the activation enthalpies of the Mg-Fe interdiffusion
158 on wadsleyite (143 kJ/mol at x = 0.90) by Kubo et al. (2004). Therefore, the annealing time at 1473
159 K was set to be greater than three times the shortest annealing time (1 h) at 1673 K. At 1473 K, the
160 samples were also expected to be in chemical equilibrium because of the longer annealing time.
161 Indeed, the K_D values determined in this study at 1473 K are also nearly identical. Katsura and Ito
162 (1989) studied the phase relation of olivine and its high-pressure polymorphs up to 21 GPa at 1873
163 K and 1473 K using quench experiments. These K_D values in Katsura and Ito (1989) are consistent
164 with those of this study. It can be concluded that all in-situ experiments reached chemical
165 equilibrium.

166 Figure 4 illustrates the phase relations of the polymorphs of olivine in the dry $(Mg,Fe)_2SiO_4$
167 system at various temperatures with the pressure calculated using the 3BM of MgO by Tange et al.
168 (2009). At each temperature, the binary loop between wadsleyite and ringwoodite was determined
169 using the present results of the iron-bearing compositions with Mg-endmembers determined by the
170 in-situ X-ray diffraction observation of Inoue et al. (2006) at approximately 1673 K, although
171 Suzuki et al. (2000) also determined that the phase boundary between wadsleyite and ringwoodite
172 in Mg_2SiO_4 at low temperatures (873–1273 K). The phase boundary determined by Inoue et al.

(2006) was suitable to adopt as the fixed point of the binary loop in this study. As shown in Figure 4, there is a discrepancy between the Mg endmember by Suzuki et al. (2000) and the binary loop in this study because of the large extrapolation of temperature in the Mg endmember while the binary loop in this study is nearly consistent with that of Inoue et al. (2006). Figure 4a and c shows that the pressures and compositional dependence of the phase boundary loop determined by Katsura and Ito (1989) are inconsistent with those in this study. These differences are probably caused by imprecise estimations of pressure during the quench experiments implemented by Katsura and Ito (1989). Akaogi et al. (1989) and Frost (2003) estimated the phase boundary of olivine polymorphs through thermodynamic calculations, as also shown in Figure 4. The compositional dependence on the binary loop is nearly consistent with the calculations reported by Akaogi et al. (1989) and Frost (2003), although the absolute pressure is different from their results. Thermochemical properties of the Fe_2SiO_4 component in wadsleyite may vary considerably because of the limited compositional range of Fe in this mineral. Thermodynamic calculation (Akaogi et al., 1989; Frost, 2003) of the phase boundary loop between wadsleyite and ringwoodite may involve considerable uncertainties, particularly regarding precise determination of the pressure boundary. Pressure determination by in-situ X-ray diffraction can be more reliable in determining the phase boundary.

Figure 4b and c also shows the pressure of the phase boundary loops of the olivine and its polymorphs under wet conditions. The phase boundary loops under wet conditions in previous studies (Inoue et al., 2010a; b; Chen et al., 2002; Frost and Dolejš, 2007) were recalculated using

192 the chemical composition of the olivine and its polymorphs under dry conditions. Chen et al. (2002)
193 and Inoue et al. (2010b) showed no evidence of a pressure difference at the Mg-endmember
194 between dry and wet conditions. However, Frost and Dolejš (2007) argued a pressure drop on the
195 phase boundary of olivine and wadsleyite under wet condition. Chen et al. (2002) and Inoue et al.
196 (2010b) performed experiments using only the Mg-endmember composition in an AuPd capsule to
197 determine the transitional pressure of the Mg-endmember, while Frost and Dolejš (2007) reported
198 experimental results of an Fe-bearing sample used as a pressure indicator in the Al_2O_3 capsule,
199 which is a quite hard material. The discrepancy in the pressure drop between these previous studies
200 might have been caused by a difference in the pressure indicator and/or capsule materials. In the
201 Fe-bearing system, the binary loop between olivine and wadsleyite shifted to a lower pressure under
202 wet condition (Chen et a., 2002), whereas that between wadsleyite and ringwoodite shifted to higher
203 pressure (Inoue et al., 2010a; b). As a result, the stability field of wadsleyite broadened under wet
204 condition. This could have been caused by the higher water solubility of wadsleyite among its
205 polymorphs and water partitioning among its polymorphs under wet condition (e.g., $D_{Wd/Ol} \sim 5$ by
206 Chen et al., 2002; $D_{Wd/Rw} \sim 2$ by Inoue et al., 2010). In contrast, the pressure difference in the binary
207 loops between dry and wet conditions decreases with increasing temperature from 1473 K to 1673
208 K. In addition, the water solubility of wadsleyite decreases with increasing temperature above 1467
209 K (Demouchy et al., 2005). The temperature dependence of the binary loops would be influenced
210 by the water solubility of the minerals. Recently, the presence of ferric iron in wadsleyite and

ringwoodite has been well known (Forst and McCammon, 2009; Mrosko et al., 2015). The stability field of wadsleyite tends to become wider with increasing ferric iron under oxidized conditions. However, to discuss the quantitative effects of ferric iron on the binary loops at each temperature, available data are not sufficient.

Implications for the 520-km seismic discontinuity

Figure 5 shows the phase relations of the olivine composition coexisting with garnet in the pyrolite model under dry and wet conditions assuming 1550–1650 K for the mantle potential temperature. McKenzie and Bickle (1988) estimated the mantle potential temperature below the mid ocean ridges to be 1550 K or higher, from the composition of mid-ocean ridge basalt (MORB). Geochemical study (Herzberg et al., 2007) and another study combining seismology and petrology (Courtier et al., 2007) have also suggested that the potential temperature at the mid-ocean ridges is 1623 ± 50 K. The mantle geotherm would be calculated as an adiabatic temperature gradient except for the surface and bottom regions in which heat flow is controlled by thermal conduction. The adiabatic temperature gradient (dT/dz) in terms of pressure (or depth) is expressed as follows:

$$\mathrm{dT}/dz = \alpha g T / C_p \quad (1)$$

where α is the thermal expansion coefficient, g is the gravity constant, T is the temperature, and C_p is the specific heat capacity at a constant pressure. The C_p of each mineral has been summarized by Akaogi et al. (1989). In addition, the adiabatic temperature profile in the mantle changes during

phase transitions because of the latent heat. The change in temperature caused by the latent heat is described as follows:

$$\mathrm{d}T_{\mathrm{latent}} = T\mathrm{d}V(\mathrm{d}P/dT)/Cp \quad (2)$$

where $\mathrm{d}T_{\mathrm{latent}}$ is the change in the temperature caused by latent heat, $(\mathrm{d}P/dT)$ is the Clapeyron slope of the phase transition, and $\mathrm{d}V$ is the volume change resulting from the phase transition. Suzuki et al. (2000) and Inoue et al. (2006) reported a Clapeyron slope of 6.91 MPa/K and 4.11 MPa/K for the wadsleyite-ringwoodite phase transition, respectively. The $\mathrm{d}V$ was calculated by the equation of the state of wadsleyite and ringwoodite by Liu et al. (2009) and Nishihara et al. (2004), respectively. Using these values, the change in temperature resulting from latent heat was calculated to be 43–26 K. To calculate the mantle geotherm, 26 K was used because the results of this study agree well with those of Inoue et al. (2006). We used the latent heat (60 K) for the olivine-wadsleyite phase transition by Katsura et al. (2004).

The seismic reflection plane formed by the olivine-wadsleyite phase boundary corresponds to the plane where the ratio of olivine to wadsleyite is 1:2 (Stixrude, 1997). From the adiabatic temperature gradient of 1550 to 1650 K for the potential temperature proposed by previous studies, the depth of the reflection plane under dry condition was estimated to be 407–419 km at a temperature of 1754–1867 K as shown in Figure 5. The 410-km seismic discontinuity is globally observed as a depth ranging between 411 km and 418 km (Gu et al. 1998; Flanagan and Shearer, 1998), corresponding to the phase boundary between olivine and wadsleyite under dry condition. In

the presence of H_2O, the phase boundary shifts to a shallower depth with decreasing temperature. However, within the expected temperature range (1754–1867 K) at 410 km depth, the effect of water on the phase boundary could be very small because the water solubility of wadsleyite decreases with increasing temperature (Demouchy et al., 2005). Even under wet conditions, the depth of the phase boundary at a 1550–1650 K potential temperature is still consistent with the 410-km discontinuity.

The depth of the seismic reflection plane caused by the phase transition between wadsleyite and ringwoodite under dry condition was calculated to be 500–514 km depth at a temperature of 1850–1950 K. Compared to the olivine-wadsleyite binary loop, the binary loop between wadsleyite and ringwoodite is much thicker and thus it is more difficult to detect it as a seismic discontinuity. The effective width of the binary phase transition was estimated to be 20–22 km with K_D = 0.63 at 1873 K based on Stixrude (1997). This effective width, which is three times larger than that of the olivine-wadsleyite phase boundary by Katsura et al. (2004), can reflect a seismic P wave of approximately 0.25 Hz (Stixrude 1997). The wadsleyite-ringwoodite binary loop is much broader than the olivine-wadsleyite phase boundary for seismic observations. Under wet condition at 1673 K, the depth of the phase boundary is greater (~13 km) than that under dry condition while the effect of water on the olivine-wadsleyite binary loop decreases with increasing temperature. The pressure interval of the wadsleyite-ringwoodite binary loop can decrease with increasing temperature. Mrosko et al. (2015) also suggested that the depth of the wadsleyite–ringwoodite phase transition deepened (~13 km corresponding to ~0.5 GPa) with oxidation conditions from the Fe-FeO buffer to Re-ReO_2

buffer at 1473 K under wet condition. There is a possibility that the transitional pressure between wadsleyite and ringwoodite increases under an oxidation state assuming a small temperature effect on oxygen fugacity. The 520-km seismic discontinuity (Gossler and Kind, 1996; Deuss and Woodhouse 2001) has been confirmed in some regions (e.g., India and central Asia) but has been found to be absent in other regions (e.g., the northeastern Pacific Ocean and northern Atlantic Ocean). In addition, analysis using a longer period shear wave (Deuss and Woodhouse, 2001; Tian et al., 2016), which allows for detection of broader phase transitions, suggests two seismic discontinuities at 500 and/or 560 km instead of one 520-km seismic discontinuity (e.g., under North Africa, North America, and Indonesia). The 500-km seismic discontinuity can be explained by the shallower wadsleyite-ringwoodite phase transition under dry and Mo-MoO_2 buffer conditions. On the other hand, chemical heterogeneity including water and oxygen fugacity of the mantle transitional zone would remain unchanged over the geological time scale, even under conditions of fastest hydrogen self-diffusion (Sun et al., 2015; 2018). When the mantle transition zone has heterogeneous water content and oxygen fugacity, the depth of the wadsleyite-ringwoodite phase boundary could be deeper than that under dry and reducing conditions (Mo-MoO_2 buffer). Therefore, the seismic discontinuity of the depth from 500 km to 520 km can be explained by the wadsleyite-ringwoodite phase boundary with water and oxygen fugacity heterogeneities. At approximately 560-km depth, there are a few minor candidates that may cause the observed seismic discontinuity, e.g., the exsolution of Ca-perovskite from garnet (Ita and Stixrude, 1992; Saikia et al., 2008), which is among

287 the major constitute minerals in MORB (Saikia et al., 2008).

288

289 **Acknowledgements**

290 We would like to thank Toshihiro Suzuki for many helpful comments. This work was supported by
291 the Grant-in-Aid for JSPS Fellows (15J09669) and Grant-in-Aid for Scientific Research (B)
292 (18H01314) to NT. We are grateful to Anwar Mohiuddin for reading the manuscript and providing
293 constructive comments. We appreciate HACTO group member for their help in obtaining diffraction
294 data. The in-situ X-ray diffraction experiments implemented to precisely determine pressure were
295 conducted on the BL04B1 at SPring-8 under the approval of the JASRI (Proposal Nos. 2012B1437,
296 2013A1475, 2013B1434, 2014A1431, 2014B1400, 2015A1600, 2015B1504, 2017A1525,
297 2017B1329, and 2018A1457).

References

Akaogi, M., Ito, E., and Navrotsky, A. (1989) Olivine-modified spinel-spinel transitions in the system Mg_2SiO_4-Fe_2SiO_4 calorimetric measurements, thermochemical calculation, and geophysical application. Journal of Geophysical Research, 94, 15671-15685

Chen, J., Inoue, T., Yurimoto, H., and Weidner D.j. (2002) Effect of water on olivine-wadsleyite phase boundary in the $(Mg,Fe)_2SiO_4$ system. Geophysical Research Letters, 29, doi:10.1029/2001GL014429

Courtier,A.M., Jackson, M.G., Lawrence, J.F. Wang, Z., Aelous Lee, C., Halama, R., Warren, J.M., Workman, R., Xu, W., Hirschmann, M.M., Larson, A.M., Hart, S.R., Lithgow-Bertelloni, C., Stixrude, L., and Chen, W. (2007) Correlation of seismic and petrologic thermometers suggests deep thermal anomalies beneath hotspots. Earth and Planetary Science Letters, 264, 308-316

Demouchy, S., Deloule, E., Frost, D.J., and Keppler, H., (2005) Pressure and temperature-dependence of water solubility in Fe-free wadsleyite. American Mineralogist, 90, 1084-1091

Deuss, A., and Woodhouse (2001) Seismic Observations of Splitting of the Mid-Transition Zone Discontinuity in Earth's Mantle. Science, 294, 354-357

Dziewonski, A.D., and Anderson, D.L. (1981) Preliminary reference Earth model. Physics of the Earth and Planetary Interiors, 25, 297-356

Flanagan, M. P., and P. M. Shearer (1998) Global mapping of topography on transition zone velocity discontinuities by stacking SS precursors. Journal of Geophysical Research, 103, 2673-2692.

Frost, D.J., (2003) The structure and sharpness of $(Mg,Fe)_2SiO_4$ phase transformations in the transition zone. Earth and Planetary Science Letters, 216, 313-328

Frost, D.J., and Dolejš, D., (2007) Experimental determination of the effect of H_2O on the 410-km seismic discontinuity. Earth and Planetary Science Letters. 256, 182–195

Frost, D.J., and McCammon, C.A., (2009) The effect of oxygen fugacity on the olivine to wadsleyite transformation: Implications for remote sensing of mantle redox state at the 410 km seismic discontinuity. American Mineralogist, 94, 872–882

Gossler, J., and Kind, R. (1996) Seismic evidence for very deep roots of continents. Earth and Planetary Science Letters, 138, 1-13

Gu, Y., Dziewonski, A. M., and Agee, C. B. (1998) Global de-correlation of the topography of transition zone discontinuities. Earth and Planetary Science Letters, 157, 57- 67.

Helffrich, G. (2000) Topography of the transition zone seismic discontinuity. Reviews of Geophysics 38, 141-158.

Herzberg, C., Asimow, P.D., Arndt, N., Niu, Y., Lesher, C.M., Fitton, J.G., Cheadle, M.J., and Saunders, A.D., (2007) Temperatures in ambient mantle and plumes: Constraints from basalts, picrites, and komatiites. Geochemistry Geophysics Geosystems, 8, 2, doi:10.1029/2006GC001390

Inoue, T., Irifue, T., Higo, T., Sanehira, T., Sueda, Y., Yamada, A., Shinmei, T., Yamazaki, D., Ando, J., Funakoshi, K., and Utsumi, W. (2006) The phase boundary between wadsleyite and ringwoodite in Mg_2SiO_4 determined by in situ x-ray diffraction. Physics and Chemistry of Minerals, 33, 106-114

Inoue, T., Wada, T., Sasaki, R., and Yurimoto, H. (2010a) Water partitioning in the Earth's mantle. Physics of the Earth and Planetary Interiors, 183, 245-251

Inoue, T., Ueda, T., Yanimoto, Y., Yamada, A., and Irifune, T. (2010b) The effect of water on the high-pressure phase boundaries in the system Mg_2SiO_4-Fe_2SiO_4. Journal of Physics: Conference Series, 2015, 012101

Ita, J., and Stixrude, L., (1992) Petrology, Elasticity, and Composition of the Mantle Transition Zone. Journal od Geophysical Research, 97, B5, 6849-6866

Katsura, T., and Ito, E. (1989) The system Mg_2SiO_4-Fe_2SiO_4 at high pressures and temperatures: Precise determination of stabilities of olivine, modified spinel, and spinel. Journal of Geophysical Research, 94, 15663-15670

Katsura, T., Yamada, H., Nishikawa, O., Song, M., Kubo, A., Shinmei. T., Yokoshi, S., Aizawa, Y., Yoshino, T., Walter, M.J., and Ito, E. (2004) Olivine-wadsleyite transition in the system $(Mg,Fe)_2SiO_4$. Journal of Geophysical Research, 109, doi:10.1029/2003JB002438

Kennett, B.L.N., and Engdahl, E.R. (1991) Traveltimes for global earthquake location and phase identification. Geophysical Journal International, 105, 429-465

Kubo, T., Shimojuku, and A., Ohtani, E., (2004) Mg-Fe interdiffusion rates in wadsleyite and the diffusicvity jump at the 410-km discontinuity. Physics and Chemistry of Minerals, 31, 456-464

Liu, W., Kung, J., Li, B., Nishiyama, N., Wang, Y. (2009) Elasticity of $(Mg_{0.87}Fe_{0.13})_2SiO_4$ wadsleyite to 12GPa and 1073K. Physics of the Earth and Planetary Interiors, 174, 98–104

McKenzie D., and Bickle, M.J. (1988) The volume and composition of melt generated by extension of the lithosphere. Journal of Petrology, 29, 623-679

Morishima, E., Kato, Suto, M., Ohtani, E., Urakawa, S., Utsumi, W., Shimomura, O., and Kikekgawa, T. (1994) The phase boundary between α- and β-Mg_2SiO_4 determined by in situ X-ray observation. Science, 265, 1202-1203.

Mrosko, M., Koch-Müller, M., McCammon, C., Rhede, D., Smyth, J.R., and Wirth, R. (2015) Water, iron, redox environment: effects on the wadsleyite-ringwoodite phase transition. Contributions to Mineralogy and Petrology, 170, 9, DOI 10.1007/s00410-015-1163-2

Nishihara, Y., Takahashi, E., Matsukage, K.N., Iguchi, T., Nakayama, K., and Funakoshi, K. (2004) Thermal equation of state of $(Mg_{0.91}Fe_{0.09})_2SiO_4$ ringwoodite. Physics of the Earth and Planetary Interiors, 143-144, 33-46

Nishiyama, N., Irifune, T., Inoue, T., Ando, J. I. and Funakoshi, K. I. (2004) Precise determination of phase relations in pyrolite across the 660 km seismic discontinuity by in situ X-ray diffraction and quench experiments. Physics of the Earth and Planetary Interiors, 143, 185–199.

Saikia Ahima, Frost, D.J., Rubie, D.C., (2008) Splitting of the 520-Kilometer Seismic Discontinuity

and Chemical Heterogeneity in the Mantle. Science, 319, 1515-1518

Shearer, P.M. (1990) Seismic imaging of upper-mantle structure with new evidence for a 520-km discontinuity. Nature, 344, 121-126

Shearer, P.M., (1991) Constrains on upper mantle discontinuity from observations of long-period reflected and converted phases. Journal of Geophysical Research, 96, 18147-18182

Speziale S., Zha, C., Duffy, T.S., Hemley, R.J. and Mao, H. (2001) Quasi-hydrostatic compression of magnesium oxide to 52 GPa: Implications for the pressure-volume-temperature equation of state. Journal of Geophysical Research, 106, 515-528

Stixrude, L., (1997) Structure and Sharpness of phase transitions and mantle discontinuities. Journal of Geophysical Research, 102, B7, 14835-14852

Sun, W., Yoshino, T., Sakamoto, N., Yurimoto, H. (2015) Hydrogen self-diffusivity in single crystal ringwoodite: Implications for water content and distribution in the mantle transition zone. Geophysical Research Letters, DOI: 10.1002/2015GL064486

Sun, W., Yoshino, T., Sakamoto, N., and Yurimoto, H., (2018) Supercritical fluid in the mantle transition zone deduced from H/D interdiffusion of wadsleyite, Earth Planet. Sci. Lett., 484, 309-317

Suzuki A., Othtani, E., Morishima, H., Kubo, T., Kanbe, y., and Kondo, T. (2000) In situ determination of the phase boundary between wadsleyite and ringwoodite in Mg_2SiO_4. Geophysical Research Letters, 27, 803-806

Tange Y., Nishihara, Y., and Tsuchiya, T., (2009) Unified analyses for P-V-T equation of state of MgO: A solution for pressure-scale problems in high P-T experiments. Journal of Geophysical Research, 114, B03208, doi:10.1029/2008JB005813

Tian, Y., Zhu, H., Zhao, D., Liu, C., Feng, X., Liu, T., and Ma, J., (2016) Mantle transition zone structure beneath the Changbai volcano: Insight into deep slab dehydration and hot upwelling near the 410km discontinuity. Journal of Geophysical Research, 121, 5794–5808, doi:10.1002/2016JB012959.

Utsumi, W., Funakoshi, K., Urakawa, S., Yamakata, M., Tsuji, K., Konishi, H., and Shimomura, O. (1998). SPring-8 beamlines for high pressure science with multi-anvil apparatus. The Review of High Pressure Science and Technology, 7, 1484-1486.

Zhang, J., and Herzberg, C. (1994) Melting experiments on anhydrous peridotite KLB-1 from 5.0 to 22.5 GPa. Journal of Geophysical Research, 99, 17729-177742

406 Figure captions

407 Figure 1. Schematic illustration of the cell assembly for the in-situ X-ray diffraction experiments.

408

409 Figure 2. Backscattered electron images of recovered samples in (a) S2840 (1473 K, 14.3 GPa, 3 h),
410 (b) S2823 (1673 K, 15.0 GPa, 1 h), and (c) S2838 (1873 K, 13.5 GPa, 1 h). Bright and dark portions
411 denote ringwoodite and wadsleyite, respectively. Wd, wadsleyite; Rw, ringwoodite.

412

413 Figure 3. Partitioning coefficient K_D values of Fe and Mg between wadsleyite and ringwoodite
414 against pressure under a dry condition and temperatures from 1473 K to 1873 K. Solid square, open
415 circle, and open diamond symbols correspond to the present study, Inoue et al. (2010a, b), and
416 Katsura and Ito (1989), respectively. Blue, green, and red color symbols indicate results determined
417 at 1473 K, 1673 K, and 1873 K, respectively.

418

419 Figure 4. Phase relations of olivine composition at (a) 1873 K, (b) 1673 K, and (c) 1473 K. The
420 black triangles are ringwoodite and wadsleyite compositions on the phase boundary loop under dry
421 conditions in this study. Black lines represent the phase boundary loop between olivine, wadsleyite,
422 and ringwoodite based on Katsura et al. (2004) and the present study using the 3BM of Tange et al.
423 (2009). The red, green, and purple lines show the phase boundary loop between wadsleyite and
424 ringwoodite under dry conditions according to Katsura and Ito (1989), Akaogi et al. (1989), and

Frost (2003), respectively. Blue circles and squares illustrate the ringwoodite and wadsleyite composition on the phase boundary loop under wet conditions according to Inoue et al. (2010a, b) recalculated using the dry phase boundary data from the present study. Blue triangles and inverse triangles indicate the ringwoodite and wadsleyite composition on the phase boundary loop reported by Inoue et al. (2010a, b) and Chen et al. (2002) recalculated using the dry phase boundary data from Katsura et al. (2004) with the 3BM of Tange et al. (2009). The blue lines represent the phase boundary loop between olivine, wadsleyite, and ringwoodite under wet condition based on Inoue et al. (2010a, b) and Chen et al. (2002). The blue region shows the compositional range of olivine $(Mg_{0.89}Fe_{0.11})_2SiO_4$, wadsleyite $(Mg_{0.90}Fe_{0.10})_2SiO_4$, and ringwoodite $(Mg_{0.905}Fe_{0.095})_2SiO_4$ proposed by Frost (2003). Ol, olivine; Wd, wadsleyite; Rw, ringwoodite.

Figure 5. Temperature profile in the normal mantle. The black solid and blue dashed lines represent the phase boundaries of the olivine-wadsleyite-ringwoodite transition under dry and wet conditions, respectively. Compositions of olivine, wadsleyite, and ringwoodite are $(Mg_{0.89}Fe_{0.11})_2SiO_4$, $(Mg_{0.90}Fe_{0.10})_2SiO_4$, and $(Mg_{0.905}Fe_{0.095})_2SiO_4$, respectively, as proposed by Frost (2003). The red bold solid lines represent geotherms in the mantle estimated from the mantle adiabatic and potential temperatures (1550, 1620, and 1650 K) under dry conditions. The green broken line represents the melting temperature curve of the dry fertile peridotite according to Zhang and Harzberg (1994). The green solid lines indicate 410, 500, 520, and 560 km in depth, which correspond to the seismic

444 discontinuity of Gu et al. (1998) and Deuss and Woodhouse (2001). Ol, olivine; Wd, wadsleyite; Rw,

445 ringwoodite.

446

This is a preprint, the final version is subject to change, of the American Mineralogist (MSA)
Cite as Authors (Year) Title. American Mineralogist, in press.
DOI: https://doi.org/10.2138/am-2019-6823

447 Table 1. Result of in-situ annealing experiments

Run.No	Load (ton)	TEL (mm)	Temperature (K)	duration (h)	Wd (Mg#)	Rw (Mg#)	K_D **	MgO V/V_0	Pressure (GPa) Tange (3BM)	Pressure (GPa) Speziale
S2932	350	5	1473	7	81.1(3)	68.4(7)	0.51(1)	0.96874(65)	12.62(15)	12.94(13)
S2840	450	4	1473	3	87.2(3)	77.8(5)	0.52(1)	0.96007(22)	14.28(5)	14.46(4)
S2947	580	5	1473	3	93.2(2)	88.3(3)	0.55(2)	0.95301(90)	15.68(23)	15.88(19)
S3323++	650->720	5	1673	8	83.2(2)	75.5(3)	0.62(1)	0.96684(53)	14.27(12)	14.47(10)
S3254	800	5	1673	6	85.1(3)	78.1(1)	0.63(1)	0.96462(57)	14.69(13)	14.90(11)
S2910	600	5	1673	2	85.3(6)	77.2(6)	0.58(3)	0.96311(56)	14.98(13)	15.19(11)
S2823	500	4	1673	1	85.5(4)	77.6(3)	0.58(1)	0.96310(88)	15.13(21)	15.20(17)
S2917	700	5	1673	2	92.9(3)	88.4(3)	0.58(2)	0.95559(89)	16.46(23)	16.75(16)
S2838	500	4	1873	1	75.1(5)	65.5(7)	0.63(2)	0.97802(79)	13.52(16)	13.89(14)
S2893	560	5	1873	1	80.6(3)	71.3(2)	0.60(1)	0.97194(85)	14.62(18)	14.85(16)
S2900	660	5	1873	1	81.2(5)	73.0(5)	0.63(2)	0.96997(61)	14.98(13)	15.21(11)
S2901	800	5	1873	2	84.5(2)	77.3(5)	0.62(2)	0.96582(84)	15.76(19)	16.00(16)
S2849	650	4	1873	1	93.3(2)	89.6(2)	0.61(1)	0.95447(82)	17.98(21)	18.26(17)
S3255*	650	5	1673	1	82.1(4)	73.5(4)	0.61(2)			
S3255+					81.3(4)	72.2(4)	0.60(1)			
a5K3134*	360	5	1673	1	82.5(6)	72.6(3)	0.56(2)			
a5K3134+					83.3(7)	74.3(7)	0.58(3)			

448 *: Fo80 powder was used as stating materials.

449 +: Mixture of Fo97 and Fo70, which bulk composition is Fo80, was used as stating material.

450 **: $K_D = \left(X_{Fe}^{Wd}/X_{Mg}^{Wd}\right)/\left(X_{Fe}^{Rw}/X_{Mg}^{Rw}\right)$

451 ++: Pressure was kept larger than pressure just after reached at a desired temperature using addition compression from 650 to 720 ton.

452 a: 5K press, which is the [111] type multi-anvil press was used.

Figure 1

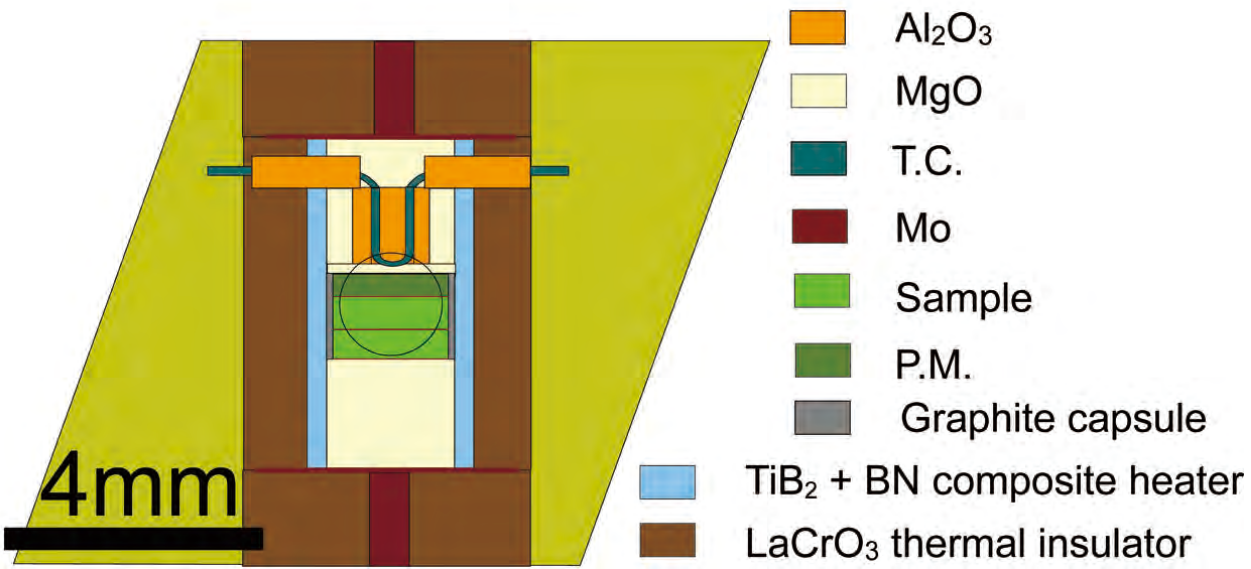
4mm
Al_2O_3
MgO
T.C.
Mo
Sample
P.M.
Graphite capsule
TiB_2 + BN composite heater
$LaCrO_3$ thermal insulator

Figure 2

(a) 1473 K, 14.3 GPa, 3 h, Mg# = 80

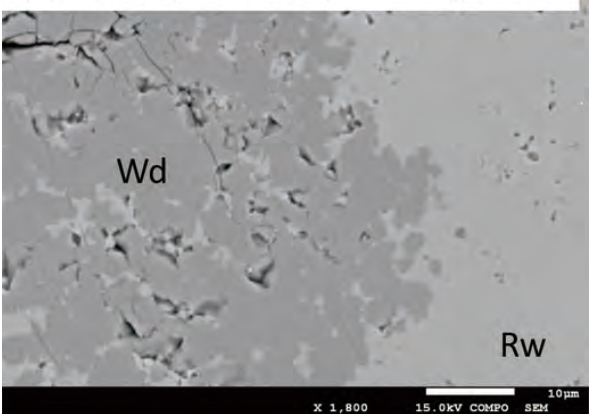

(b) 1673 K, 15.0 GPa, 1 h, Mg# = 80

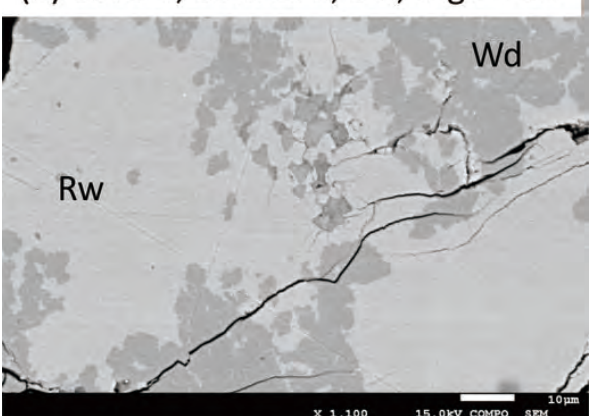

(c) 1873 K, 13.5 GPa, 1 h, Mg# = 70

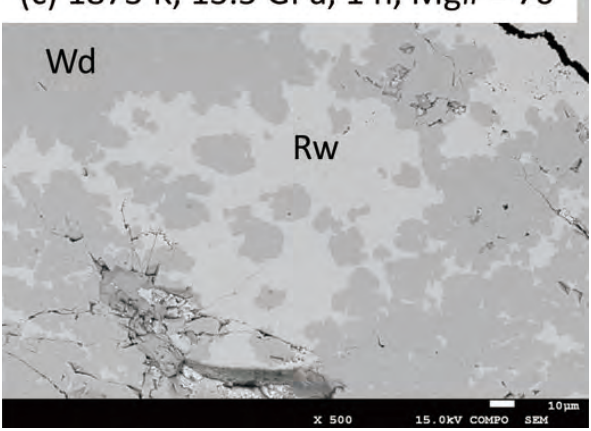

Figure 3

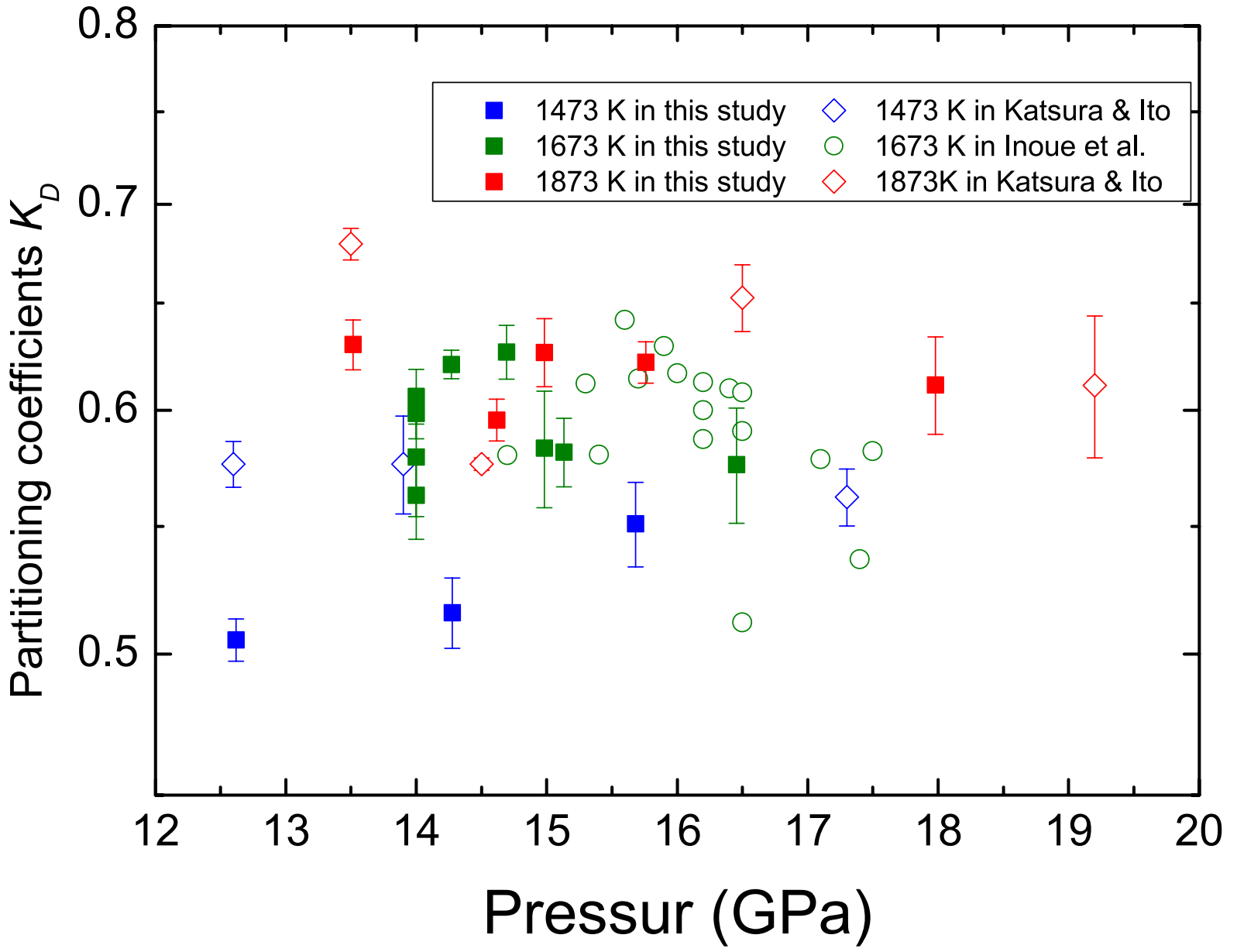
0.8
0.7
0.6
0.5
Partitioning coefficients K_D
12
13
14
15
16
17
18
19
20
Pressur (GPa)
1473 K in this study
1673 K in this study
1873 K in this study
1473 K in Katsura & Ito
1673 K in Inoue et al.
1873K in Katsura & Ito

Figure 4

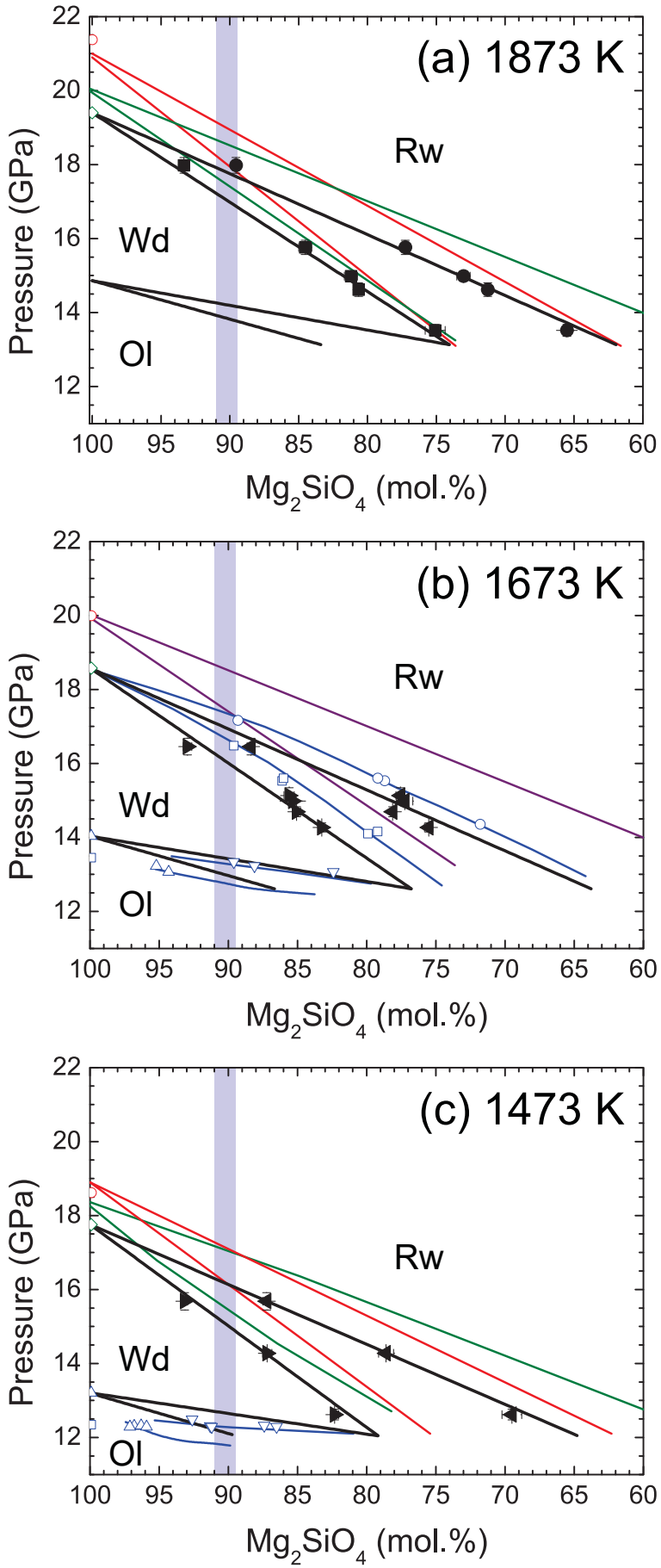
(a) 1873 K
Rw
Wd
Ol
Pressure (GPa)
22
20
18
16
14
12
100
95
90
85
80
75
70
65
60
Mg2SiO4 (mol.%)
(b) 1673 K
Rw
Wd
Ol
Pressure (GPa)
Mg2SiO4 (mol.%)
(c) 1473 K
Rw
Wd
Ol
Pressure (GPa)
Mg2SiO4 (mol.%)

Figure 5

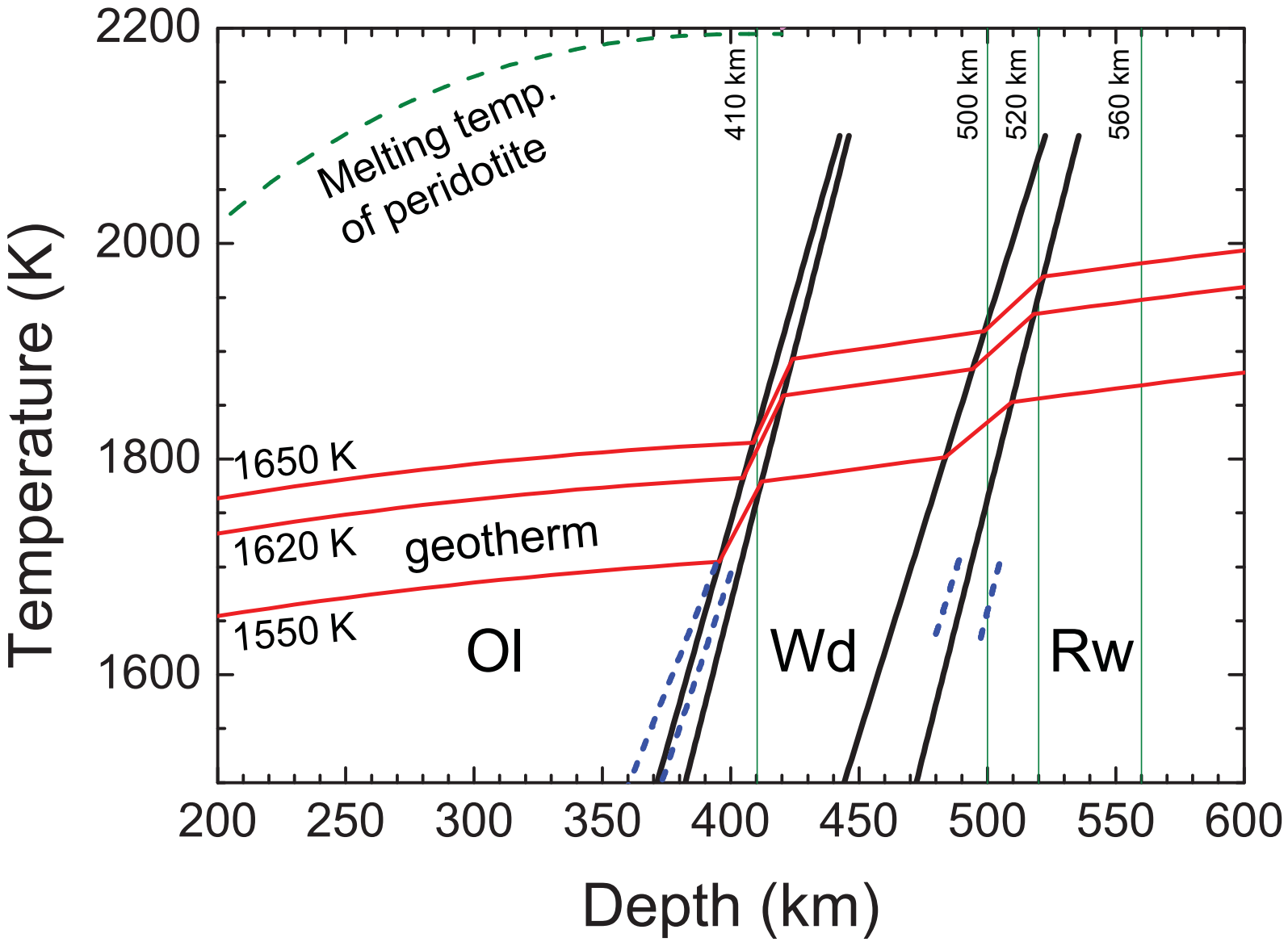
2200
2000
1800
1600
Temperature (K)
200
250
300
350
400
450
500
550
600
Depth (km)
Melting temp.
of peridotite
410 km
500 km
520 km
560 km
1650 K
1620 K
1550 K
geotherm
Ol
Wd
Rw